J Solid State Electrochem (2009) 13:1291–1296
DOI 10.1007/s10008-008-0675-3

ORIGINAL PAPER

Pitting behavior on super 13Cr stainless steel in 3.5% NaCl solution in the presence of acetic acid

Z. F. Yin · W. Z. Zhao · W. Tian · Y. R. Feng · C. X. Yin

Received: 10 June 2008 / Revised: 29 July 2008 / Accepted: 8 September 2008 / Published online: 23 September 2008

Abstract The pitting behavior was investigated on super 13Cr stainless steels in 3.5% NaCl solution in the presence of HAc. The electrochemical measurements including potentiodynamic polarization, electrochemical impedance spectroscopy (EIS), and chronoamperometric experiments were carried out, as well as the SEM surface analysis. The parameters such as E_{corr} and I_{corr} were obtained by fitting technique. Moreover, the equivalent circuit model was applied in the analysis of Nyquist plots, and ZsimWin software was used to analyze the EIS data. The results indicate that the pitting corrosion is accelerated with increasing the amounts of HAc. In addition, pitting nucleation and growth mechanisms were described in this work.

Keywords Super 13Cr stainless steel · Acetic acid · SEM · Pitting

Introduction

Pitting corrosion of metals and alloys is one of the main causes of material failure in industrial systems [1]. It is difficult to control pitting corrosion due to its complex nature. Pitting corrosion comprises two main processes: pit nucleation and pit growth. Some authors have considered that pit initiation is attributed to the breakdown of the passive film layer [2, 3] caused by random fluctuations at local sites. After pit nucleation occurs, the pit can repassivate immediately or grow and then repassivate. In general, this process is regarded as metastable pitting. If a metastable pit can grow indefinitely, it becomes a stable pit [1].

As known, acidic gases such as carbon dioxide and volatile organic acids co-produced with the hydrocarbons constitute the corrosive environment in real oil–gas system. Acetic acid (HAc) is one of the most abundant volatile organic acids and can be present in concentrations up to several thousand parts per million in the aqueous phase. Field experience shows that HAc is one of most significant factors in the localized corrosion attacks in gas-condensate pipelines [4]. When a gaseous phase of HAc is present in oil–gas pipelines, it, in addition to CO_2, dissolves into the aqueous solution. The HAc then dissociates into hydrogen and acetate ions, which can be expressed as

$$HAc \rightleftarrows H^+ + Ac^- \quad (1)$$

Because HAc is a stronger acid than carbonic acid, it is the main source of hydrogen ions when the two acid concentrations are similar. The acetate ions can form iron acetate based on the reaction with iron as follow

$$Fe + 2HAc \rightleftarrows Fe(Ac)_2 \quad (2)$$

The literatures on CO_2 corrosion in presence of HAc were published in past years. Some studies reported increased corrosiveness in presence of HAc [5–8], whereas others reported that HAc works as an inhibitor leading to the lower corrosion rate [9, 10].

It is still complicated to understand and describe the pitting corrosion despite of much endeavor on it. The

Z. F. Yin (✉) · W. Z. Zhao
School of Materials Science and Engineering,
Xi'an Jiaotong University,
Xi'an 710049, People's Republic of China
e-mail: yinzhifu919@sohu.com

Z. F. Yin · W. Tian · Y. R. Feng · C. X. Yin
The Key Laboratory for Mechanical and Environmental Behavior of Tubular Goods, Tubular Goods Research Center, CNPC,
Xi'an 710065, People's Republic of China

mechanism of the pit nucleation and growth in HAc/CO_2 environments is seldom studied. On the other hand, the investigation on the effect of HAc/CO_2 focused on carbon steel except for few instances on stainless steel, especially in high temperature. To further understand and describe pitting corrosion, electrochemical measurements techniques and scanning electron microscopy (SEM) were utilized to provide insight into behavior of super 13Cr stainless steel in 3.5% NaCl solution in the presence of HAc.

Materials and methods

Material preparation All samples were made from super 13Cr stainless steel with the chemical composition (wt.%): C 0.013, Si 0.14, Mn 0.7, P 0.016, S 0.00072, Cr 13.34, Mo 0.63, Ni 5.33, Fe Balance. The samples were embedded in epoxy resin with an exposed working area of 1.766 cm^2. A new sample was always used for each experiment and prior to the electrochemical tests; the working surfaces were wet-ground with SiC sand papers up to 1,200 grit and rinsed with distilled water and absolute alcohol. All experiments were carried out in 3.5% NaCl solutions, containing different amounts of HAc (0, 1,000, 3,000, and 5,000 ppm), saturated with O_2-free CO_2 gas at high temperature (90 °C).

Electrochemical measurements The pitting corrosion experiments were carried out by potentiodynamic polarization and electrochemical impedance spectrum (EIS) techniques in a conventional three-electrode cell. The chronoamperometric experiments at fixed potential were carried out using EG&G PAR Model 273A potentialstat–galvanostat. The recording of time dependent curves was performed as follows: the samples were activated at −1.0 V for 5 min and subsequently, the potential was stepped to the preselected potential (−0.2 V) and then the current response was monitored vs. time. The counter electrode was a pair of graphite and the reference electrode a saturated calomel electrode (SCE). All potentials were referred to SCE. The ZsimpWin software was used to analyze the EIS data. The EIS measurements were carried out at E_{corr} using 10 mV amplitude perturbation and a frequency range of 100 to 5 mHz. Potentiodynamic polarization was conducted by means of linear sweep technique, with a sweep rate of 0.5 mV s^{-1}. Before each experiment, the corrosive solution was deaerated by pure N_2 for 2 h and then CO_2 was bubbled in solution for 1 h, respectively then, the quantities of HAc were poured into the deaerated solution. During the process of experiments, the CO_2 bubbled successively through the solution. The test temperature was controlled at 90 °C.

SEM analysis SEM was utilized to investigate microstructures and characteristics of the corrosion pits. Before SEM measurement, the polarized samples were cleaned in absolute alcohol in order to removing the surface contamination.

Results and discussion

Potentiodynamic polarization

Figure 1 shows the potentiodynamic polarization curves obtained on super 13Cr stainless steel in 3.5% NaCl solution with different amounts of HAc saturated with CO_2 at 90 °C. It can be easily seen that the corrosion potential (E_{corr}) increases with the amounts of HAc, i.e., the corrosion potential shifts more positive value, as shown in Table 1. Furthermore, obvious passivation regions occur in the anodic branches of all polarization curves as illustrated in Fig. 1. However, the anodic Tafel slope (b_a) is smaller than those in the presence of HAc, which means that HAc plays a role in corrosion process. Compared to the anodic branches, the cathodic branches of the polarization curves almost have the same change trend. It is clear that the addition of HAc increases the cathodic limiting currents and, thus, can enhance the potential corrosiveness, which is in good agreement with the result by Crolet et al. [5]. In addition, corrosion current density (I_{corr}) increases with the amounts of HAc as shown in Table 1. It, thus, indicates that the corrosion attack increases with increasing the amounts of HAc. From all passive regimes easily discerned in the anodic branch of the polarization curves, it can be concluded that the corrosion process is controlled by the

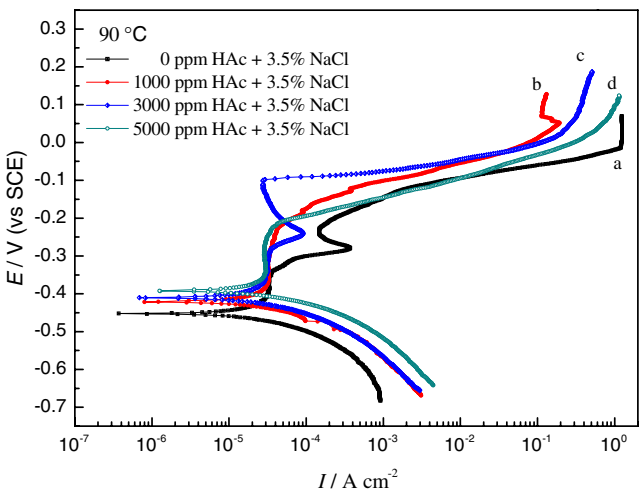

Fig. 1 The potentiodynamic polarization curves obtained at 90 °C in 3.5% NaCl solution with different quantities of HAc: *a* 0 ppm, *b* 1,000 ppm, *c* 3,000 ppm, and *d* 5,000 ppm

Table 1 Corrosion parameters obtained from polarization curves for super 13Cr stainless steel at 90 °C in sodium chloride solution with different quantities of HAc

Parameters	0 ppm	1,000 ppm	3,000 ppm	5,000 ppm
E_{corr} (V)	−0.451	−0.419	−0.407	−0.387
b_a (V dec^{-1})	0.069	0.145	0.132	0.156
b_c (V dec^{-1})	−0.049	−0.055	−0.060	−0.054
I_{corr} (μA cm^{-2})	11.35	14.87	16.64	19.52

combined effects between anodic dissolution and cathodic diffusion.

Chronoamperometric experiments

In order to get some insight into the surface processes, the time dependence of the current density (i) on the duration (t) of application of a polarizing potential is of special interest. The laws correlating to the film growth was represented in investigation by Long G et al. [11]. They considered that the repassivation process was described stepwise by the relationship $i=At^s$. If the oxidation films formed are assumed to be homogeneous, the dc current density i through the layer is determined by the resistance R of a unit film area according to Ohm's law $i=U/R$, where U is the potential difference. R is proportional to the film thickness D, i.e., $R=aD$. Therefore, the current density correlated with the thickness can be expressed by the relationship $i=U/(aD)$. In addition, D is a function of time and is assumed as the relationship $D(t) = bt^{-s} + c$. The exponent s is determined for $i(t) \sim t^s$ from log–log plots as shown in Fig. 2. Here, when the slope s=–1, it refers to a linear growth. It is usually related to the formation of a compact and good protective passive film. When the slope s=–0.5, it means a parabolic growth rate which corresponds to a process controlled by the diffusion of reactants. A slope s>0 is due to the common controlling processes between pit nucleation and pit propagation.

In Fig. 2, the $i(t)$ dependence recorded during the applied potential (−0.2 V) is shown. It can be observed that after about 100 s, the almost linear growth dominates the corrosion process (s>0) except the case for the added 5,000 ppm HAc. According to the slope s law [11], the initial layer formation is controlled by diffusion and prior to a stable pit growth the formation of oxide layer and pit nucleation proceeds competitively. However, for the case of added 5,000 ppm HAc, the typical $i(t)$ recording reveals well the competitive processes of slow breakdown and recovery of passive films after about 400 s. From the passive region in Fig. 1, it is almost in agreement with the behavior of potentiodynamic curves.

EIS measurements

Figure 3 represents the Nyquist plots at OCP obtained on super 13Cr stainless steel in 3.5% NaCl solution containing different amounts of HAc saturated with CO_2 at 90 °C. The spectra of super 13Cr stainless steel exhibit a similar behavior containing two depressed semicircles with a moderate magnitude of impedance in the intermediate or low frequency regions, which indicates a common resistant passive film formation. It is clear that the diameter of the depressed semicircle decreases with the increase of HAc which indicates the increased corrosion attack. In addition, the depressed semicircle might be due to microscopic surface roughness and presence of a porous corrosion product film as presented by Touzet [12]. The fitting parameters of impedance data obtained by using the equivalent circuit model in Fig. 4 are listed in Table 2. For the equivalent

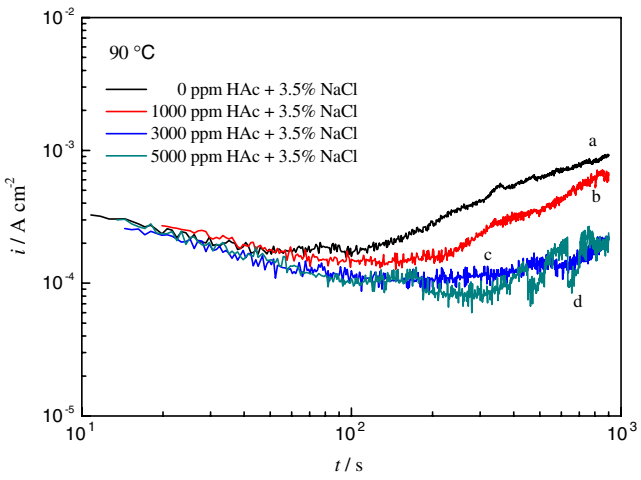

Fig. 2 Time dependent log–log plots of current density recorded in 3.5% NaCl solution with different quantities of HAc: *a* 0 ppm, *b* 1,000 ppm, *c* 3,000 ppm, and *d* 5,000 ppm

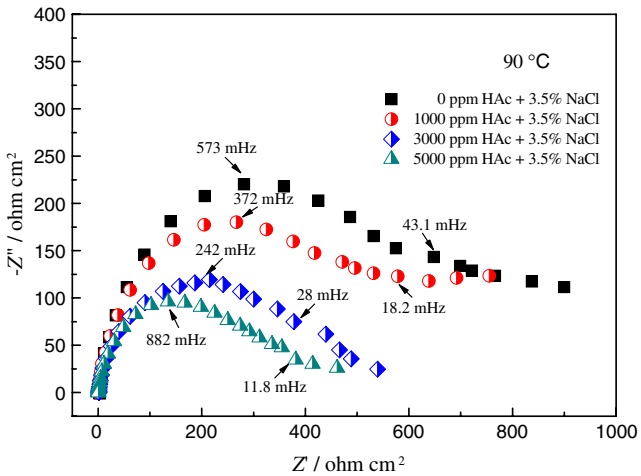

Fig. 3 The Nyquist plots obtained at 90 °C in 3.5% NaCl solution with different quantities of HAc

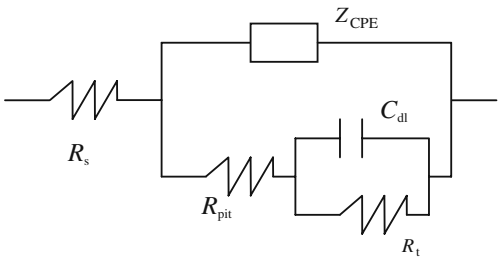

Fig. 4 The equivalent circuit corresponding to Nyquist plots for super 13Cr stainless steel

electric circuit, where R_s is the solution resistance between the working and reference electrodes, R_t and R_{pit} are charge transfer resistance of diffusion controlled reaction and the electrical resistance to the ionic current through the pits, respectively, C_{dl} represents the double layer capacitance. Besides, the impedance of the capacitance element Q is presented by the constant phase element (CPE) which is widely used as scattered circuit element in equivalent circuits when non-ideal frequency response is present. The impedance of Z_{CPE} is shown in Eq. 3 [13]

$$Z_{CPE} = A^{-1}(jw)^{-n} \tag{3}$$

where A is a proportional coefficient related with the combination of the properties between the surface and electro-active species, $j = \sqrt{-1}$, $w = 2\pi f$ is the angular frequency. While n is CPE exponent, which can be used as a gauge of surface heterogeneity.

According to the equivalent circuit model in Fig. 4, the impedances of the electrodes for all cases are given by

$$Z(\omega) = R_s + \left\{ j\omega Q + \left[R_{pit} + \left(R_t^{-1} + j\omega C_{dl} \right)^{-1} \right] \right\} \tag{4}$$

As shown in Table 2, the R_t value decreases steadily with the increase of the amounts of HAc, about two times decreasing up to 5,000 ppm HAc, which suggests the addition of HAc can enhance the corrosion attack on the electrodes. At the same time, R_{pit} values have small magnitude, so the pit nucleation and growth process is faster than the pit repair process which is available for the ionic current through the pits. The probable reason is that the uniform corrosion substitutes the localized corrosion with added HAc and the repassivation is not enough to repair the pits in passive films. The result is accordant with that of the polarization curves. In addition, the CPE exponent n from 0.40 to 0.46 demonstrates that the electrochemical corrosion process is not pure capacitance or resistance behaviour according to the investigation by Cao et al. [14] in which the CPE respectively represents capacitance (n=0, Q=R) and resistance (n=1, Q=C).

In order to fully describe the corrosion characteristics of super 13Cr stainless steel, we introduce a relaxation time τ, which can be expressed as [15]

$$\tau = \frac{1}{\omega} \tag{5}$$

While,

$$\omega = RC \tag{6}$$

Based on Eqs. 5 and 6, the relaxation times τ calculated are 4.63, 3.81, 5.07, and 7.18 s, respectively. Therefore, the relaxation time increases with the added HAc except for the 1,000 ppm HAc case which is probably induced by experiment error. The data indicates that the relaxation time can be applied to evaluate the corrosion resistance because τ is well correlated with the time of the pit repassivation.

SEM analysis

Figure 5 shows the SEM images of super 13Cr stainless steel in 3.5% NaCl solution containing different amounts of HAc saturated with CO_2 at 90 °C. By SEM technique, it is clear that the diameters of corrosion pits (D_{pit}) are respectively about 210.9, 243.6, 345.6, and 243.6 μm corresponding to the 0, 1,000, 3,000, and 5,000 ppm HAc cases, respectively. It can conclude that the diameter of corrosion pit increases with the amounts of HAc. In addition, there are more corrosion pits adjacent to the major corrosion pits on the sample surfaces with increasing HAc. It is the secondary-grown corrosion pits relating to the corrosion processes of nucleation and growth. In

Table 2 Parameters obtained from the equivalent circuit corresponding to Nyquist plots for super 13Cr stainless steel at 90 °C in 3.5% NaCl solution with different quantities of HAc

Parameters	0 ppm	1,000 ppm	3,000 ppm	5,000 ppm
R_s (Ω cm^2)	0.2129	0.1939	0.1915	0.1985
Q-Y_O (Ω^{-1} cm^{-2} s^{-1})	844.5×10^{-6}	1219×10^{-6}	1802×10^{-6}	1719×10^{-6}
Q-n	0.460	0.443	0.439	0.405
R_{pit} (Ω cm^2)	0.0288	0.0193	0.0397	0.0281
C_{dl} (F cm^2)	234.5×10^{-6}	323.7×10^{-6}	349.1×10^{-6}	296.8×10^{-6}
R_t (Ω cm^2)	921.9	810.4	565.5	469.3

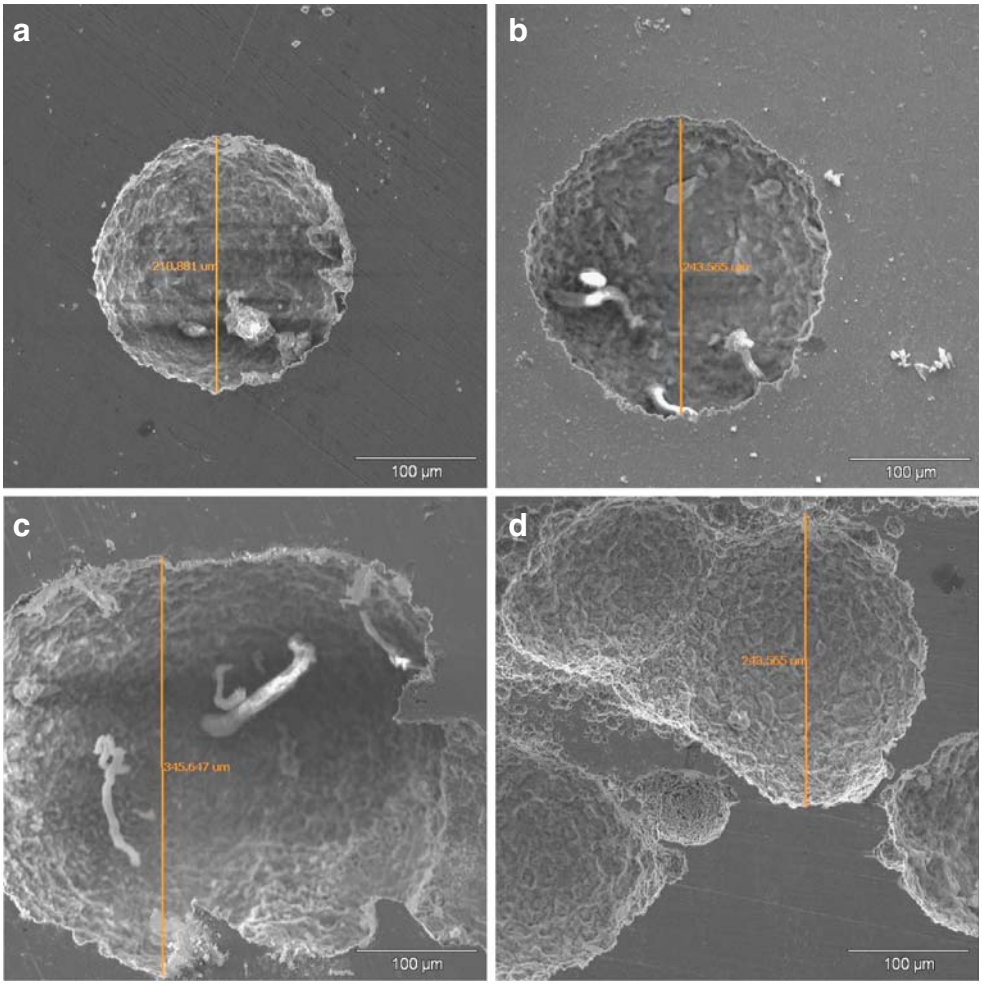

Fig. 5 The SEM pictures obtained at 90 °C in 3.5% NaCl solution with different quantities of HAc: **a** 0 ppm, **b** 1,000 ppm, **c** 3,000 ppm, and **d** 5,000 ppm. Magnification ×200

general, pitting is believed to be due to the local breakdown of the passive film which results in rapid dissolution of bare metal in the presence of aggressive ions such as chloride [16] and with the effect of acid [17].

We consider that the morphology characteristics of pitting in present work are the combination effects of between the penetration mechanism (anions such as Cl^- penetrate through the passive film to bare metal surface and react with the

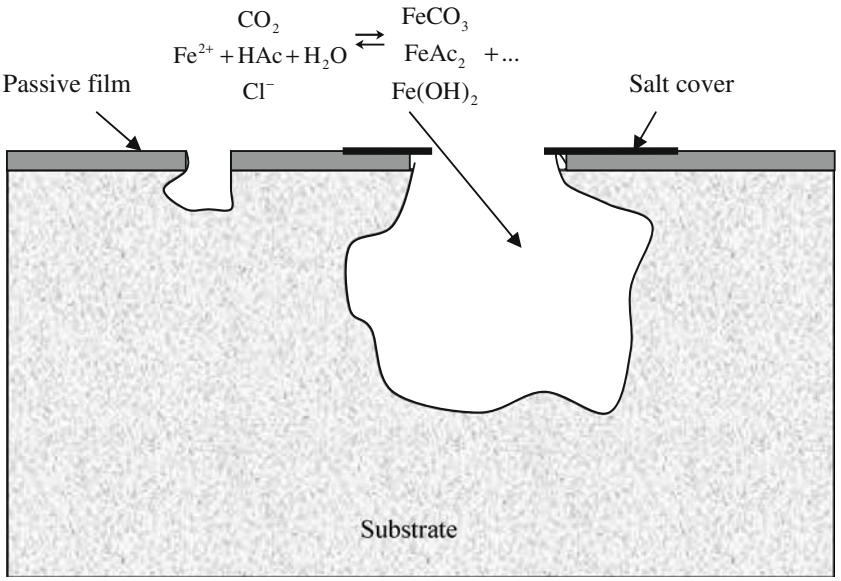

Fig. 6 The schematic picture for the pitting corrosion process in later stage of pitting growth at 90 °C in 3.5% NaCl solution with CO_2 and HAc

metal) and acid-activation mechanism (once the pit nucleation, a self-propagation or autocatalysis follows). With the corrosion process, the cation concentration increases inside the pit as the pit grows. The diffusion of metal cation reduces its concentration at the pit mouth for active dissolution; thus, this area is probably repassivated. The representative pitting characteristics is depicted in Fig. 6. The area deeper in pit, however, is still under active dissolution, and the sidewall is undercut and a small hole formed on the surface in the later stage of pit growth. The process repeats itself and more pits are formed and the pits grow into a saucer-like shape. In addition, it can be seen that the accumulation of salt cover formed at the mouth of corrosion pits. We consider that it is more difficult to repassivate when pits grow deeper by the morphologies of corrosion pits as shown in Fig. 5. The result is not in well agreement with the result from Rosenfeld [18] who found that puncturing of the salt cover leads to the repassivation of the corrosion pits. However, the pitting corrosion process is so complicated that all kinds of controversies relating to the pitting mechanisms occur. For this work, we describe the schematic picture of pitting corrosion in 3.5% NaCl solution with CO_2 and HAc as shown in Fig. 6.

As it is known, when CO_2 and HAc are present in the corrosive environment, there exist some corrosive reactions in the system relating to the cathodic reactions, which can be given as the following Eqs. 7–9

$$2CO_2 + 2H_2O + 2e \rightarrow 2HCO_3^- + H_2 \quad (7)$$

$$2HAc + 2e \rightarrow 2Ac^- + H_2 \quad (8)$$

$$2H^+ + 2e \rightarrow H_2 \quad (9)$$

Even though the acetate ions have a limited effect on the pH, because of the buffering action, they can play a significant role in the hydrogen evolution reaction which is a rate-controlling step in the corrosion reaction The H_2 evolution from HAc seems to be under activation control and diffusion control. Herein, we can compare the contributions from CO_2 and HAc to corrosion. In the past literature published, we can see that HAc is a stronger acid than carbonic acid which is not accordant with the result from D. Palmer et al. [19] obtained by calculation that the dissociation constant Ka of H_2CO_3, expressed as pKa, is 3.5 at normal temperature, i.e., lower than for HAc (pKa 4.8). Accordingly, H_2CO_3, which is the cathodic reactant in CO_2 corrosion, is a stronger acid than HAc. Therefore, it can be well recognized to the corrosion solution phases in the system with CO_2 and HAc. However, there exist a series of complicated correlations between HAc, Ac^-, H_2CO_3, HCO_3^-, and H^+ ions in the corrosive solution in presence of CO_2 and HAc to further comprehend the pitting mechanisms.

Conclusions

The tests in this work indicated that the addition of HAc increases the cathodic limiting currents and thus can enhance the potential corrosiveness. The corrosion potential (E_{corr}) shifted more positive value with the additive amounts of HAc. Corrosion current density (I_{corr}) also increased with HAc. The diameter of the depressed semicircle in Nyquist plots decreased with the increase of HAc. The initial layer formation is controlled by diffusion and prior to a stable pit growth the formation of oxide layer and pit nucleation proceeds competitively by using Time dependent log–log plots of current density. In addition, there were more corrosion pits adjacent to the major corrosion pits on the sample surfaces with increasing HAc. The morphology characteristics of pitting were the combination effects of between the penetration mechanism and acid-activation mechanism.

Acknowledgements The authors want to thank the Key Laboratory Opening Fund (No. 06A40302) of Corrosion and Protection of Tabular Goods Research Center of China National Petroleum Corporation for supports to this work.

References

1. Burstein T, Liu C, Souto RM, Vines SP (2004) Corros. Eng Sci Tech 39:25. doi:10.1179/147842204225016859
2. Frankel GS (1998) J Electrochem Soc 145:2186. doi:10.1149/1.1838615
3. Shibata T, Takeyama T (1976) Nature 260:315. doi:10.1038/260315a0
4. Gunaltun YM, Larrey D (2000) NACE paper no. 71. NACE, Houston
5. Crolet JL, Bonis MR (1983) NACE paper no.160. NACE, Houston
6. Sun Y, George K, Nesic S (2003) NACE paper no. 327. NACE, Houston
7. George K, Nesic S, de Waard C (2004) NACE paper no. 379. NACE, Houston
8. Guo XP, Chen ZY, Liu D, Bando K, Tomoe Y (2005) NACE paper no. 306. NACE, Houston
9. Hedges B, McVeigh L (1999) NACE paper no. 21. NACE, Houston
10. Gunaltun YM, Belghazi A (2001) NACE paper no. 33. NACE, Houston
11. Long G, Grandjean F (1996) Mössbauer spectroscopy applied to magnetism and materials science. Plenum, New York
12. Touzet M et al (1993) Corros Sci 34:1134. doi:10.1016/0010-938X(93)90297-T
13. Chen Y, Jepson WP (1999) Electrochim Acta 44:4453. doi:10.1016/S0013-4686(99)00160-7
14. Cao CN, Zhang JQ (2002) An introduction to electrochemical impedance spectroscopy. Science, Beijing
15. Baek JS, Kim JG, Hur DH, Kim JS (2003) Corros Sci 45:983–994. doi:10.1016/S0010-938X(02)00183-X
16. Wranglen G (1974) Corros Sci 14:331. doi:10.1016/S0010-938X(74)80047-8
17. Lott SE, Alkire RC (1989) J Electrochem Soc 136:973. doi:10.1149/1.2096896
18. Rosenfeld IL, Marshakov IK (1964) Corrosion 20:115
19. Palmer DA, van Eldik R (1983) Chem Rev 83:651. doi:10.1021/cr00058a004